Engineering Fracture Mechanics 194 (2018) 73–85

Contents lists available at ScienceDirect

Engineering Fracture Mechanics

journal homepage: www.elsevier.com/locate/engfracmech

Characterization of concrete matrix/steel fiber de-bonding in an SFRC beam: Principal component analysis and *k*-mean algorithm for clustering AE data

Sena Tayfur[a], Ninel Alver[a,*], Saeed Abdi[b], Selçuk Saatcı[c], Amir Ghiami[d]

[a] Ege University, Faculty of Engineering, Department of Civil Engineering, 35100 Bornova, Izmir, Turkey
[b] University of Zanjan, Faculty of Engineering, Department of Mechanical Engineering, 38791 Zanjan, Iran
[c] Izmir Institute of Technology, Faculty of Engineering, Department of Civil Engineering, 35430 Urla, Izmir, Turkey
[d] School of Materials Science and Technology, Chemistry Department, University of Parma, 43121 Parma, Italy

ARTICLE INFO

Keywords:
Steel fiber reinforced concrete
De-bonding
Acoustic emission (AE)
Clustering
Principal component analysis (PCA)

ABSTRACT

Steel fibers have been used in concrete structures to increase the tensile strength and ductility of concrete. Fibers bridging cracks reduce micro cracking and improve post-cracking strength in concrete. Propagation of damage in a fiber reinforced concrete member occurs by concrete matrix cracking and widening of these cracks, which is accompanied by de-bonding of steel fibers from the concrete matrix. Fiber de-bonding is the main factor affecting the post-peak behavior of these members. Therefore, distinguishing the matrix cracking and fiber de-bonding mechanisms is important in nondestructive structural health monitoring methods. This study is focused on characterizing steel fiber/matrix de-bonding events apart from concrete matrix cracking sources in acoustic emission (AE) method. Two reinforced concrete beams, one of which included steel fibers within the concrete matrix, were tested under three point bending and monitored by AE. Afterwards, Principal Component Analysis (PCA) was applied to AE data and the failure mechanisms were clustered for characterization of steel fiber/matrix de-bonding. Finally, different AE features of these clusters were evaluated and applicable AE parameter distributions, which are useful to clarify steel fiber de-bonding mechanisms, were revealed.

1. Introduction

Concrete is a widely used construction material, which has a tensile strength significantly lower than its compressive strength. Typically steel bars are used in concrete structures to overcome this weakness and provide ductility to structural concrete members. In addition to steel bars, natural, synthetic, glass or steel fibers are also used in concrete structural elements due to their function in bridging the cracking surfaces transferring tensile stresses, which significantly increases post-cracking ductility of concrete [1]. Tensile stresses carried across cracks decrease crack widths in such fiber reinforced structural members, increasing their ductility and bending stiffness [2–8].

Steel fibers have its advantages over other types of fibers due to their higher stiffness, higher strength and high aspect ratio. Therefore, they are commonly used in numerous applications where cracking of concrete is of primary concern, such as industrial slabs, precast structural members and tunnel linings [2]. Mechanical properties of concrete members reinforced with steel fibers depend on fiber dosage, geometry, bonding with concrete and orientation of fibers as well as characteristics of concrete matrix

* Corresponding author.
E-mail address: ninel.alver@ege.edu.tr (N. Alver).

https://doi.org/10.1016/j.engfracmech.2018.03.007
Received 20 September 2017; Received in revised form 6 March 2018; Accepted 7 March 2018
Available online 08 March 2018

[3,9,10].

In order to clarify these mechanisms and determine the damage level of a structure, various test techniques can be used. Generally, these techniques investigate the damaged state of the member and they need sampling for testing. However, it is important to make a decision before any visible damage takes place. Nondestructive testing methods have been developed for this purpose, providing information about the state of overall system without inflicting any damage on the structure. Acoustic Emission (AE) is one of the nondestructive test techniques providing information about crack progresses even at low load levels. The method is based on the detection of elastic waves propagating in the body generated by energy discharge due to fracture [11]. By capturing these waves with sensors, location and time of origin of fracture can be determined. A number of studies have been carried out to identify fracture mechanisms and fracture energies of concrete and steel fiber reinforced concrete members [2,12–18]. The studies about steel fiber reinforced concrete conclude that AE activity is proportional to the fiber content [12].

Based on AE parameters, it is possible to determine the failure mechanism of the concrete by various analyses [19–21]. In this paper, cluster analysis was applied to AE parameters which provides grouping objects according to their similarities such that the similarities in the same group are high while in different groups the similarities are low [22]. *K*-means is one of the most popular and widely used clustering algorithms due to its reliability and simplicity. The method aims to separate observations into the clusters in which distance between mean and the observations in the cluster are minimized. In the iterative algorithm, firstly, the clusters are initialized with random centers. Then the distances of each input to the cluster's center are computed and the inputs are assigned to their nearest cluster. Finally, the centers of the clusters are recalculated. Last two stages are repeated until the centers of the clusters converge [23].

Studies show that PCA is an effective tool to correlate clusters using various data [24–29]. Rossiter [30] used principal component regression on infrared spectra of concrete samples in order to predict their properties. Godin et al. [31] conducted tensile tests on pure resin samples and on polyester/glass fiber unidirectional composites and identified mechanisms as matrix cracking and interfacial de-cohesion by *k*-means. Precisely discriminating signals associated with de-bonding and signals associated with fiber failure was difficult, but the researchers regarded the results as encouraging. Ning et al. [32] and Milovanovic and Pecur [33] applied PCA to infrared thermography results obtained in concrete. Calabrese et al. [34] tested AE behavior of concrete beams under four-point-bending and determined their clusters. For this purpose, they used PCA and Kohonen's self-organizing map clustering algorithms and compared them with traditional AE parameter analysis procedures. They pointed out that the methods require the development of validation procedure to optimize a correct interpretation of great amounts of data. Calabrese et al. [35] used AE to monitor hydrogen assisted stress corrosion cracking of post-tensioned strands and distinguished three subsequent damage phases using cumulative hits. Then they confirmed the results with PCA and self-organizing maps and proved them to be particularly effective in identifying the evolution and intensity of corrosion damage on steel wires in the monitored post-tensioned concrete beam. Saliba et al. [36] carried out an experimental investigation to characterize local damages and physical mechanisms underlying creep of concrete. As a result of the study, the researchers obtained two clusters for basic creep and three clusters for desiccation creep. Fotouhi et al. [37] used AE and PCA to investigate different failure mechanisms of delamination in glass/epoxy composite laminates. They found out matrix cracking and fiber/matrix de-bonding dominantly and some fiber breakages took place. Anay et al. [38] monitored cement paste specimens by AE under compression test and classified active crack growth by PCA. They acquired three stages as crack micro crack initiation, stable and unstable crack growth by separating AE data into clusters. Roundi et al. [39] investigated static and fatigue behavior of glass/epoxy composite laminates with AE and classified accumulated damages as matrix cracking, fiber/matrix de-bonding, delamination and fiber breakage by *k*-means method and PCA. Researchers observed matrix micro-cracks as the most dominant damage mechanism and detected few signals representing the fibers breaking.

In this study, differently from the abovementioned studies, it was aimed to distinguish steel fiber/matrix de-bonding events apart from concrete matrix cracking by cluster analysis based on PCA using AE features. For this purpose, two reinforced concrete beams, one of which included steel fibers within concrete matrix, were tested under three point bending and monitored by acoustic emission. Afterwards, cluster analyses were applied to AE data for characterization of steel fiber/matrix de-bonding.

2. Acoustic emission (AE)

According to ASTM E 1316 [40], Acoustic Emission (AE) is defined as an event producing transient elastic waves by releasing of a number of local sources in materials under stress. In this context, AE can be considered as a microseism. In the method, stress wave is produced at a source by applied stress. The vibration reaches to sensors located at the surface and is transformed into an electrical signal. Then it arrives to pre-amplifier, filter, power amplifier, and counters, respectively.

In AE procedure, the first purpose is to determine the location of a crack. It can be determined by using the time difference between each sensor and the source. It is also possible to make some predictions about the fracture by using AE parameters as shown in Fig. 1. Here, "amplitude" is the maximum voltage on an AE waveform and it is a significant parameter with regard to constitution of the perceptibility of AE activity. AE amplitude is directly related to magnitude of an event. During the test, a definite amplitude value is specified in order to pick ambient noise. This parameter is defined as "threshold". The number of pulse passing the threshold is "count". "Rise time" is an elapsed time between first and last counts passing the threshold. The area under the rectified signal envelope is named as "MARSE (Measured Area under the Rectified Signal Envelope)", which is the energy.

3. Principal component analysis (PCA)

Principal component analysis (PCA) is an approach to discern the patterns in data. Through that, the similarities and differences in

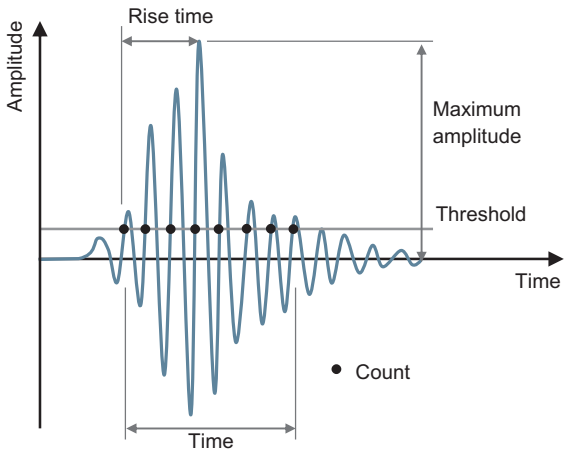

Fig. 1. AE signal parameters.

the dataset can be highlighted. Since graphical representation and efficient numerical analysis in dataset with high dimensionality bring difficulties, PCA can be used as a reliable tool for reducing dimensionalities of the data without losing much information.

Introducing PCA to a set of data consists of several steps including calculation of covariance and eigenvectors of the dataset which has already been put into a matrix. The detailed steps are represented in the following tree diagram [41].

The dataset must be formed into a matrix of data. In order to increase the efficiency of the algorithm, the mean value of each dimension must be subtracted from the corresponding dimension. The resulted dataset will have the zero-mean value. The product of the Sections 3,4 and 5 are actually a matrix of vectors in which an eigenvalue can be calculated for each vector. The vectors with the highest eigenvalues are the desired vectors which can produce the final data set by simply taking the transpose of the vector and multiplying it on the left of the original dataset (Eq. (1)):

$$Final\ data = (Raw\ Feature\ Vector) \times (Raw\ Data) \tag{1}$$

where *Raw Feature Vector* is the matrix of the eigenvectors with the highest corresponding eigenvalues ordered from top to bottom. *Raw Data* is the mean-adjusted data transposed. The *Final Data* which comprises a stronger pattern relative to the primary dataset can be taken for desirable analysis. Algorithm of PCA is shown in Fig. 2.

As mentioned in Section 2, acoustic emission signals are comprised of several features that each one of them carries some information of the originating source. In order to perform a precise dimensionality reduction by applying PCA analysis, all possible known features must be taken into account. In this study, primary vectors for initiating PCA analysis are considered to be the peak frequency, root mean square error (RMS), amplitude, duration, count, rise time, and absolute energy.

3.1. k-mean clustering algorithm

Among the unsupervised clustering algorithms, k-mean is well known for its simplicity and feasibility. This algorithm follows a straightforward way to classify a given set of data into a certain number of clusters. First step is to define the centroids in which the number of the centroids is depending on the number of clusters that have been presumed. The primary positions of the centroids must be as far as possible relative to each other to increase the precision of the analysis. The next step is to associate each point to the nearest centroid. When no point is pending, the initial classification has been completed. This point forward, the new positions of the centroid must be recalculated until the so called objective function, *J*, becomes minimized as calculated using Eq. (2) [42].

$$J = \sum_{j=1}^{k} \sum_{i=1}^{n} \|x_i^{(j)} - c_j\|^2 \tag{2}$$

where $\|x_i^{(j)} - c_j\|^2$ is a specific length between point $x_i^{(j)}$ and the cluster center c_j, which is an indicator of the n^{th} point from their respective cluster centers. In other words, the last step would be repeated until centroids move no longer and a separation of the objects into classes for which the distances are minimized is obtained.

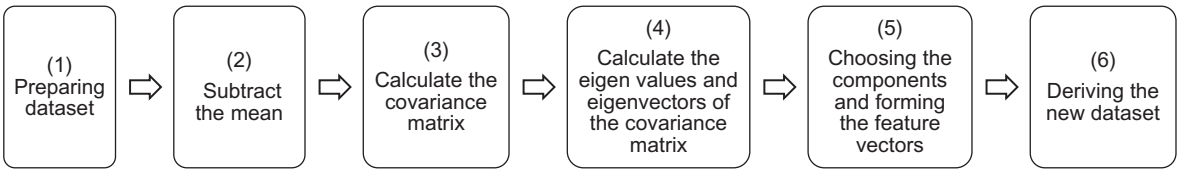

Fig. 2. Algorithm of principal component analysis.

3.2. Silhouette function

Silhouette function is an efficient method for evaluation of the consistency of a set of data within the corresponding classes. To be precise, Silhouette can be applied as a tool for investigating how well a set of data have been clustered into a certain given number of clusters by use of a certain clustering method. The Silhouette value is a measure of how similar an object is to its own cluster compared to other clusters [43].

Through the following equation, Silhouette value can be calculated as follows:

$$s(i) = \frac{b(i)-a(i)}{\max\{a(i),b(i)\}} \tag{3}$$

In which the $a(i)$ is the average dissimilarity of i with all other data within the same cluster. $b(i)$ is the lowest average dissimilarity of i to any other cluster, of which i is not a member. Therefore, as the similarity of data in each cluster increases, the equation would yield a higher average value which indicates the validity of the number of clusters predefined as well as proper assignment of each data to the clusters. The value calculated by Silhouette function is a number between 0 and 1.

4. Experimental program

4.1. Design of the specimens

In the experimental program, two reinforced concrete beams were produced and were tested under three-point-bending. The specimens were designed with 2Ø8mm longitudinal steel reinforcement at both top and bottom and without shear stirrups. While one of the specimens was the reference beam (RC Beam), the other (SFRC Beam) was strengthened with 1% steel fibers in volume fraction. The beams were 150 × 250 × 2350 mm in dimension with 2000 mm span. Test setup and section details of the specimens are presented in Fig. 3.

4.2. Materials

Concrete used for production of the specimens was included in C25/30 strength class and cement type was CEM II B-M (L-W) 42.5 R. Water/cement ratio of the mixture and maximum aggregate sizes were 0.65 and 16 mm, respectively. Moreover, in order to enhance the workability of the concrete, which was reduced due to steel fibers, superplasticizer was added into the mixture. Mechanical properties of plain and steel fiber reinforced concrete are given in Table 1. Steel reinforcing bars were tested in tension to obtain the mechanical properties. Characteristic strength and elastic modulus of longitudinal reinforcing bars were determined as 420 MPa and 200 GPa, respectively.

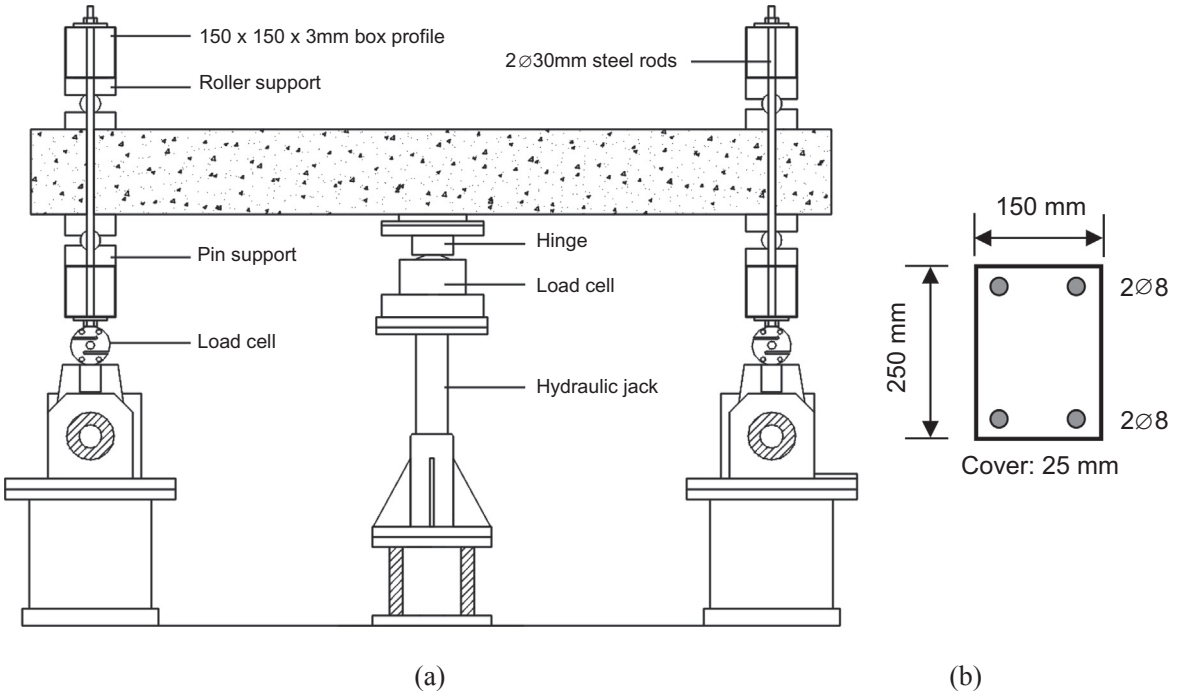

Fig. 3. (a) Test setup, (b) Section details of the specimens.

Table 1
Mechanical properties of plain and steel fiber reinforced concrete.

Volume fraction of steel fiber (%)	f'c (MPa)[a]		f'ts (MPa)[b]	f'tf (MPa)[c]
	28-days	Test day	Test day	
0	33.80	42.40	2.30	3.45
1	35.20	45.40	3.50	5.25

[a] Compressive strength of concrete.
[b] Splitting tensile strength of concrete.
[c] Flexural tensile strength of concrete.

Bekaert Dramix RC 8060 BN hooked steel fibers were used for reinforcing of concrete. Characteristics of the steel fiber are presented in Table 2.

4.3. Experimental setup

The specimens were tested under three-point-bending. A vertical monotonic load was applied to the beams at their bottom mid-spans systematically and slowly in order to observe crack propagations better. Thirteen potentiometers were used to monitor displacements. Seven AE sensors having 150 kHz frequency (R15, PAC) were attached to different locations of the specimens by silicon grease to detect AE waves. In order to record AE data, an 8-channel DiSP AE system by Mistras Holding was used. A threshold level of 40 dB was set. HDT, PDT and HLT values were configured as 800, 200 and 200 microseconds, respectively. All AE hits were used in the analyses. Locations of the sensors are shown in Fig. 4.

5. Results and discussion

5.1. Mechanical results

Three-point-bending tests were performed on both specimens. During the tests, mechanical properties and AE results were obtained. Load vs. mid-span deflection curves of the specimens are shown in Fig. 5.

Fig. 6 shows crack propagations of the test specimens. First cracks of RC Beam were observed at 19 kN load level. By increasing the load, these cracks and other invisible ones propagated. New cracks became visible when the load was 26.1 kN. The specimen reached to its ultimate load capacity of 30.4 kN when deflection was 43 mm. After this, applied load decreased while deflections increased. The specimen failed by four major flexural cracks when the displacement was measured 52.1 mm. First cracks of SFRC Beam occurred at 35.5 kN load level. Increase in load gave rise to new cracks. The specimen reached to its ultimate load capacity of 42.2 kN, when deflection was 26 mm. Finally, it collapsed by a major flexural crack when the displacement was 41.5 mm. SFRC Beam showed higher ultimate resistance in contrast to the reference specimen, RC Beam. This is a consequence of presence of the steel fibers.

5.2. Cluster analysis results

As given in Fig. 7, the dimensionality reduction of the AE matrixes of features was successfully accomplished by application of PCA analysis. This fact is referred to the total values of the variances of PCA1 and PCA2 in each specimen which are obtained more than 90%. PCA1 and PCA2 are said to be the new features in the novel coordinate system calculated by PCA analysis. In other words, the two new features (PCA1 and 2) belonging to each specimen can be replaced by initial multiple features introduced in the primary coordinate system. It is clear that numerical calculation can be more easily applied for two variants (PCA 1 and 2) in comparison to multiple variants.

It is important to bear in mind that, the number of clusters which different classes of events can be attributed to, must be approximated based on the primary knowledge; then, according to the assumption, the clustering must be performed, and the validity of the result can be examined by Silhouette function. For two different specimens, clustering has been tried for different number of clusters ranging from 2 to 8. Obtained results are calculated and represented in Fig. 8. The maximum obtained value is said to be the most reliable cluster number in which the data must be put. According to Fig. 8, the most appropriate values were obtained as 2 and 3

Table 2
Characteristics of the steel fiber.

Properties	Remarks of Bekaert Dramix RC 8060 BN
Length (mm)	60
Diameter (mm)	0.75
Tensile strength (MPa)	1050

Test Specimen	Sensor	X (m)	Y (m)	Z (m)
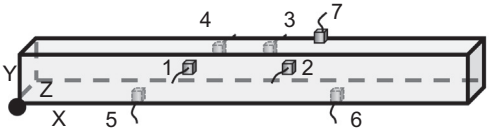	1	0.895	0.125	0.000
	2	1.430	0.125	0.000
	3	1.440	0.120	0.150
	4	0.955	0.115	0.150
	5	0.865	0.000	0.080
	6	1.490	0.000	0.075
	7	1.380	0.250	0.085

Fig. 4. Locations of AE sensors.

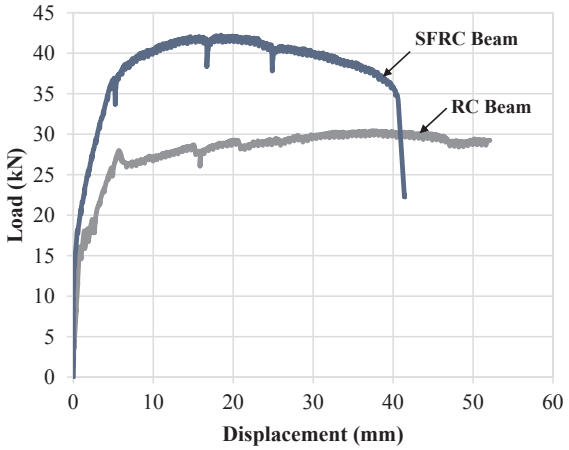

Fig. 5. Load vs. deflection responses of the test specimens.

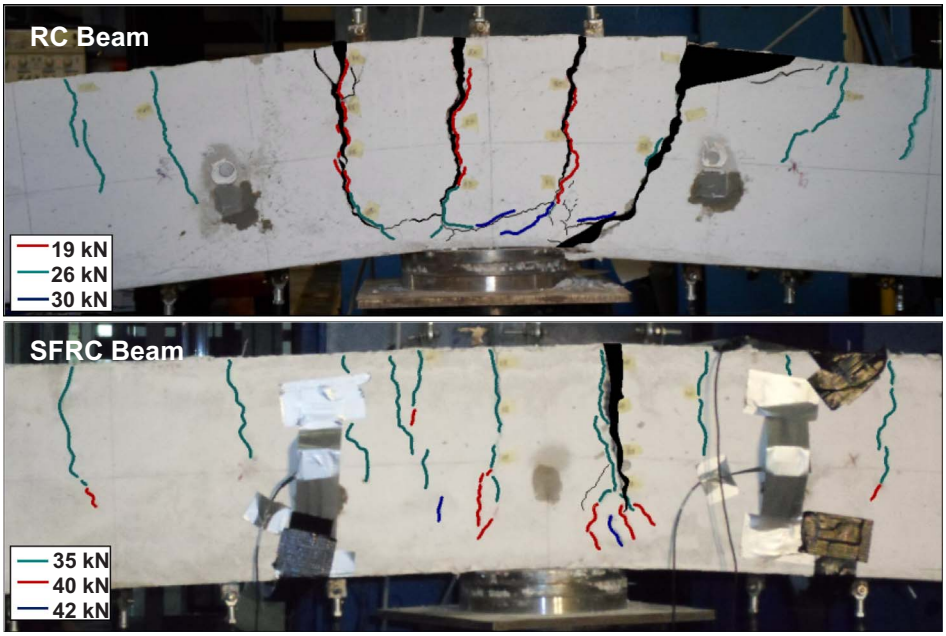

Fig. 6. Crack propagations in the test specimens.

for RC and SFRC specimens, respectively.

While the main purpose of this study is to discriminate the AE signals related to steel fiber/matrix de-bonding failure mechanism, the data set of RC Beam was assumed to be a single cluster so that the influence of the steel fiber addition could be easily recognized

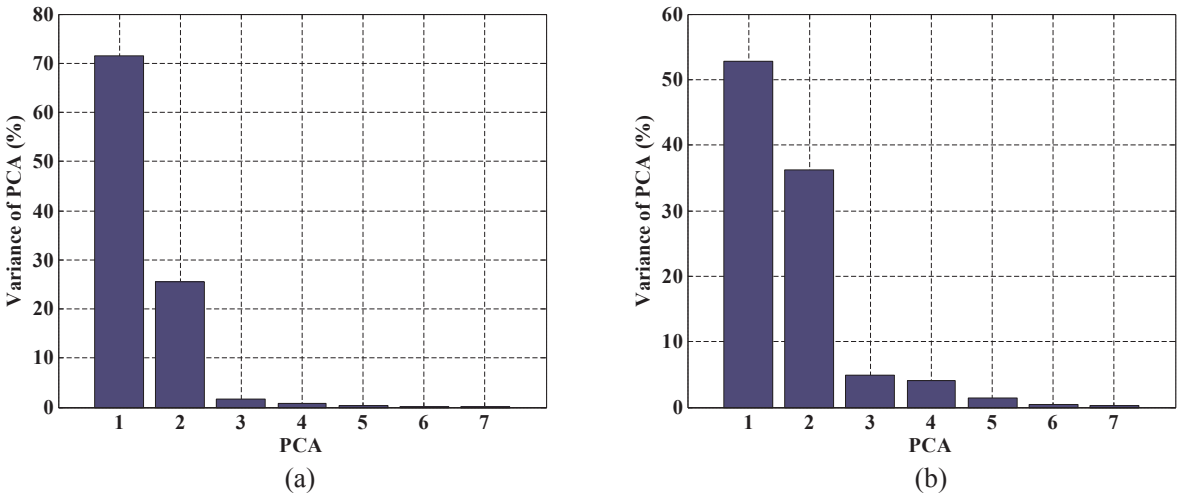

Fig. 7. Variances of PCA values: (a) RC Beam, (b) SFRC Beam.

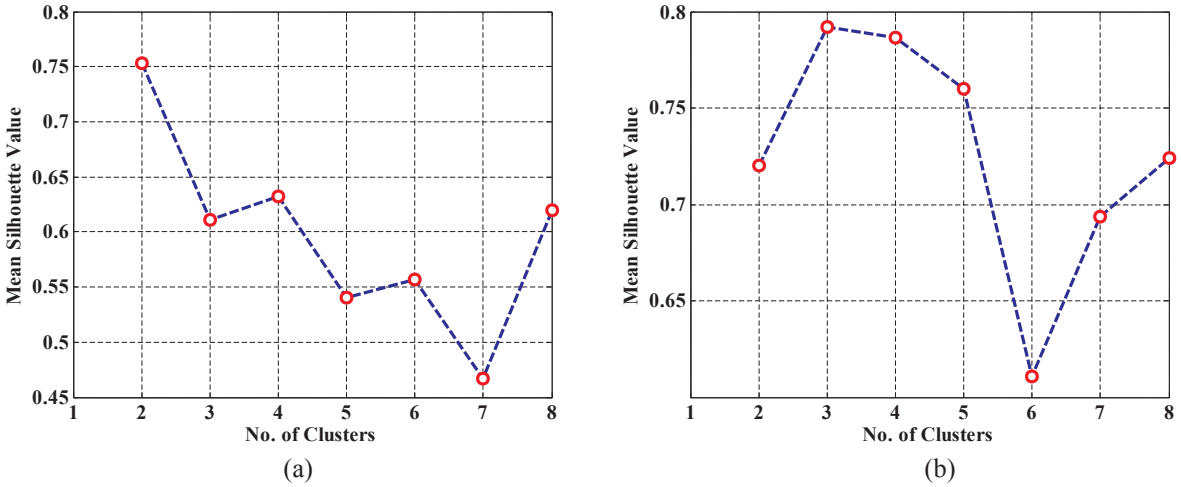

Fig. 8. Silhouette function values: (a) RC Beam, (b) SFRC Beam.

while analyzing the data set of SFRC Beam. Distribution of the data set related to RC Beam is given in Fig. 9 (left side).

Considering the clustering result of SFRC Beam (Fig. 9, right), it can be seen that, the data set pattern of RC Beam is exactly repeated in the data set pattern of SFRC Beam with approximately 0.7 unit shifted to right and a bit counterclockwise rotation. The changes in position of the pattern is due to the normalizing of the initial matrixes of features and the clustering algorithm implementation, hence, does not incorporate any practical significances. As a result, it can be concluded that the data set pattern which is representing a failure mechanism recognized in RC Beam has also been identified in SFRC Beam.

The top graph in Fig. 9 is representing a part of data distributed in PCA1 and PCA2 coordinates which appears in both specimens, thus, it was called as the repetitive pattern. This pattern is attributed to series of events that occurred in both RC and SFRC specimens. It was considered as a black box since the authors were interested in the specific event that is exclusive to the SFRC specimen, which found to be the steel fiber debonding from concrete matrix.

On the other hand, it can be seen that, the single cluster in RC Beam (Fig. 9, left) is divided into two separate clusters (clusters 1 and 3) in SFRC Beam (Fig. 9, right). This fact could be attributed to the micro-failure mechanisms the RC Beam may experience whilst loading. Occurrence of micro-failure mechanisms in RC Beam could be originated from the cement and mortar composition and the size of aggregates as well as the quality of concrete production procedure.

While the main objective of this study was to identify the steel fiber/matrix de-bonding failure mechanism, the occurrence of micro-failure mechanisms will be ignored and the clusters 1 and 3 (in RC Beam) will be integrated into one cluster. Final schemes of the *k*-means clustering results are shown in Fig. 10.

According to Fig. 10, the main distinguishing point of the RC Beam and SFRC Beam clustering result is the presence of the second cluster in Fig. 10(b). While the main difference between two specimens is the usage of steel fibers, it can be easily concluded that the second cluster seen in Fig. 10(b) is attributed to the steel fiber/matrix de-bonding. It should be kept in mind that the total assumable

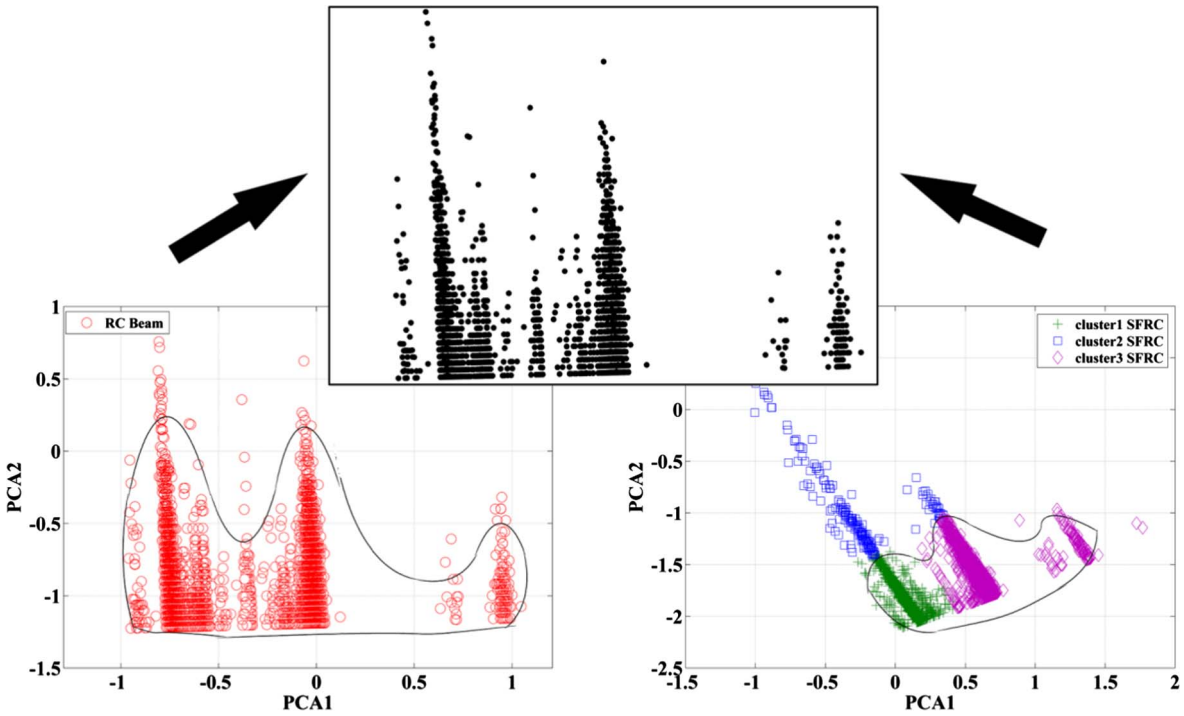

Fig. 9. Patterns of clusters in *k*-means clustering results: (left) RC Beam, (right) SFRC Beam.

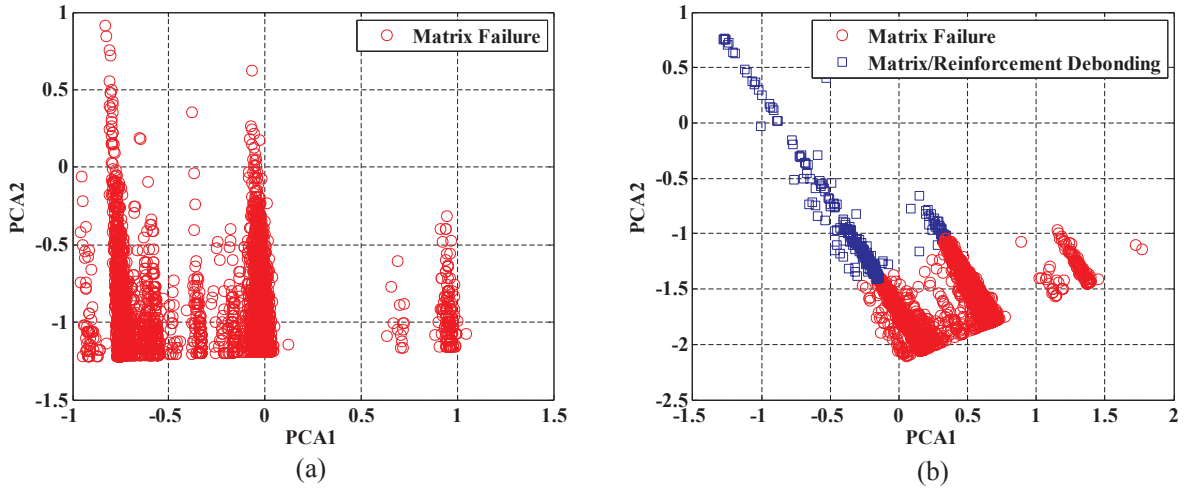

Fig. 10. Final schemes of the *k*-mean clustering results: a) RC Beam, b) SFRC Beam.

failure mechanisms in such steel fiber reinforced specimens are matrix failure, fiber failure and steel fiber/matrix de-bonding.

5.2.1. Relative distribution of acoustic emission features

Relative distribution patterns of rise time vs. count are shown in Fig. 11. Based on the clustering results, the repeating part in both distribution patterns is correspondent to Cluster 1. The distribution pattern for RC Beam is concluding an extra area (Cluster 2) which is attributed to steel fiber/matrix de-bonding failure mechanism.

It can be seen that, “rise time vs. count” distribution pattern can clearly reveal the changes in acoustic emission data with the addition of steel fiber.

Distribution patterns for duration and amplitude combination are given in Fig. 12. It can be seen that, Cluster 2 in SFRC Beam distribution pattern has been clearly separated from Cluster 1. Due to that, a similar discussion given for rise time vs. count distribution pattern can be introduced for duration and amplitude combination. “Duration vs. amplitude” has also shown good capability in identifying steel fiber/matrix debonding failure mechanism.

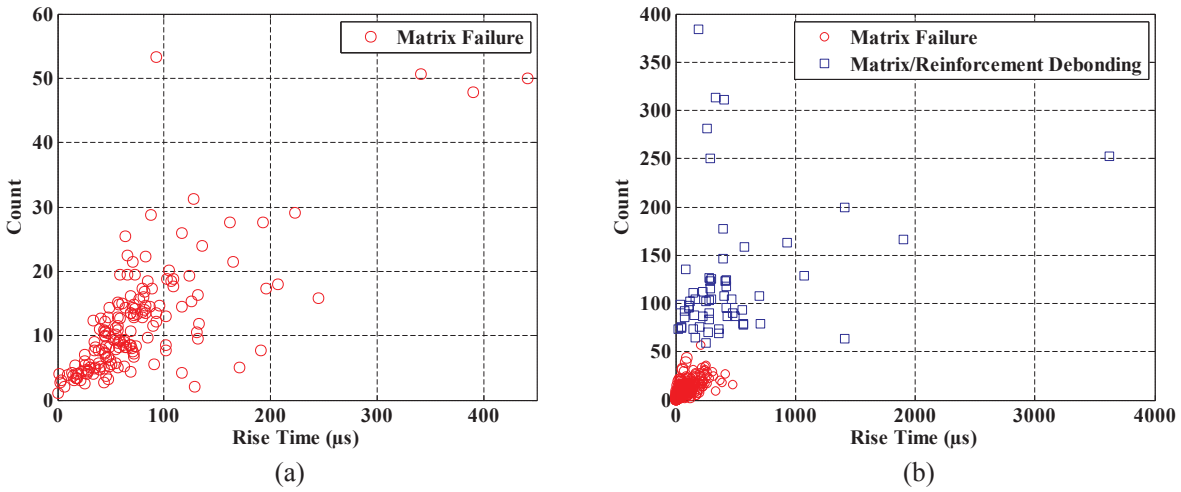

Fig. 11. Distribution patterns of rise time vs. count: (a) RC Beam, (b) SFRC Beam.

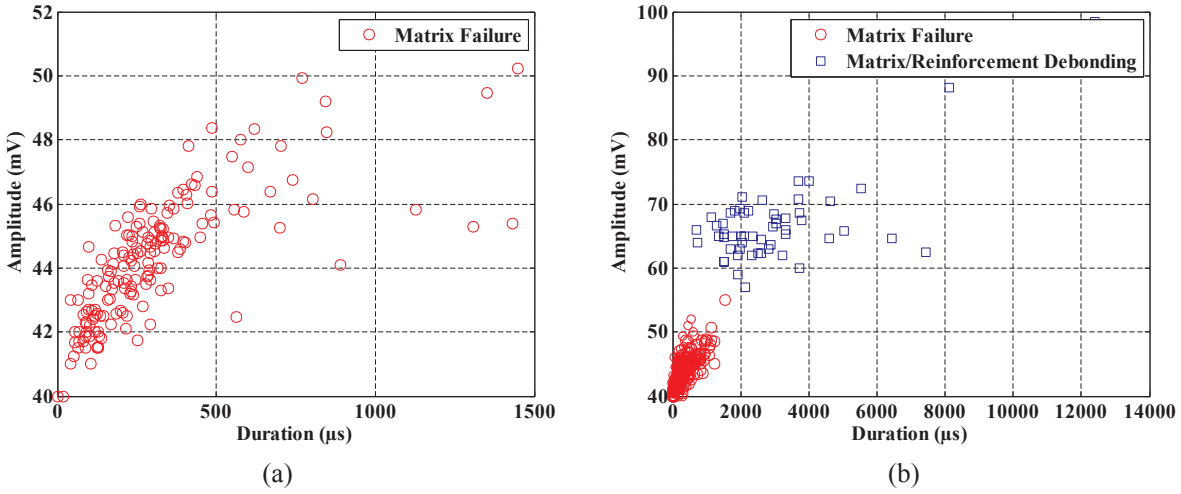

Fig. 12. Distribution patterns of duration vs. amplitude: (a) RC Beam, (b) SFRC Beam.

Unlike the two latter combinations of features, peak frequency vs. amplitude and rise time vs. duration could not sufficiently separate the clusters of two failure mechanisms which are matrix failure and matrix/reinforcement de-bonding. As can be seen in Fig. 13, clusters are stacked together and the boundary cannot easily be distinguished. Hence, these two combinations cannot be considered as trustable way of identifying the de-bonding failure mechanism.

Based on the aforementioned results, it can be concluded that among the whole acoustic emission features and their combinations, rise vs. count and duration vs. amplitude have the highest capability in determining the failure status of the concrete and steel fiber reinforced concrete. The obtained results are in accordance with results acquired by *k*-means clustering algorithm.

Magnitude ranges of the acoustic emission features for both failure mechanisms (clusters) are given in Fig. 14. The summary of the magnitudes are shown in Table 3. The differences in the ranges of features' magnitudes can easily be recognized. As presented in Table 3, the magnitudes of the AE features for Cluster 2 in SFRC Beam have egregious differences from magnitudes of Cluster 1. This is where the values for Cluster 1 in SFRC Beam are very similar to the values for single cluster of RC Beam which confirms that there exists an identical failure mechanism in both specimens which is matrix failure and the other failure mechanism (Cluster 2) is exclusive for SFRC Beam.

Considering the magnitude ranges of the acoustic emission features of two failure mechanisms, it can be concluded that, steel fiber/matrix de-bonding failure mechanism produces high magnitude acoustic emissions relative to matrix failure. This is a critical point of distinguishing the signals emitted during occurrence of the failure mechanisms.

5.2.2. AE cumulative energy analysis

In order to obtain a more profound understanding of influence of steel fiber/matrix de-bonding on behavior of the reinforced concrete beam, time vs AE cumulative energies and the corresponding loads are presented in Fig. 15. A meaningful difference

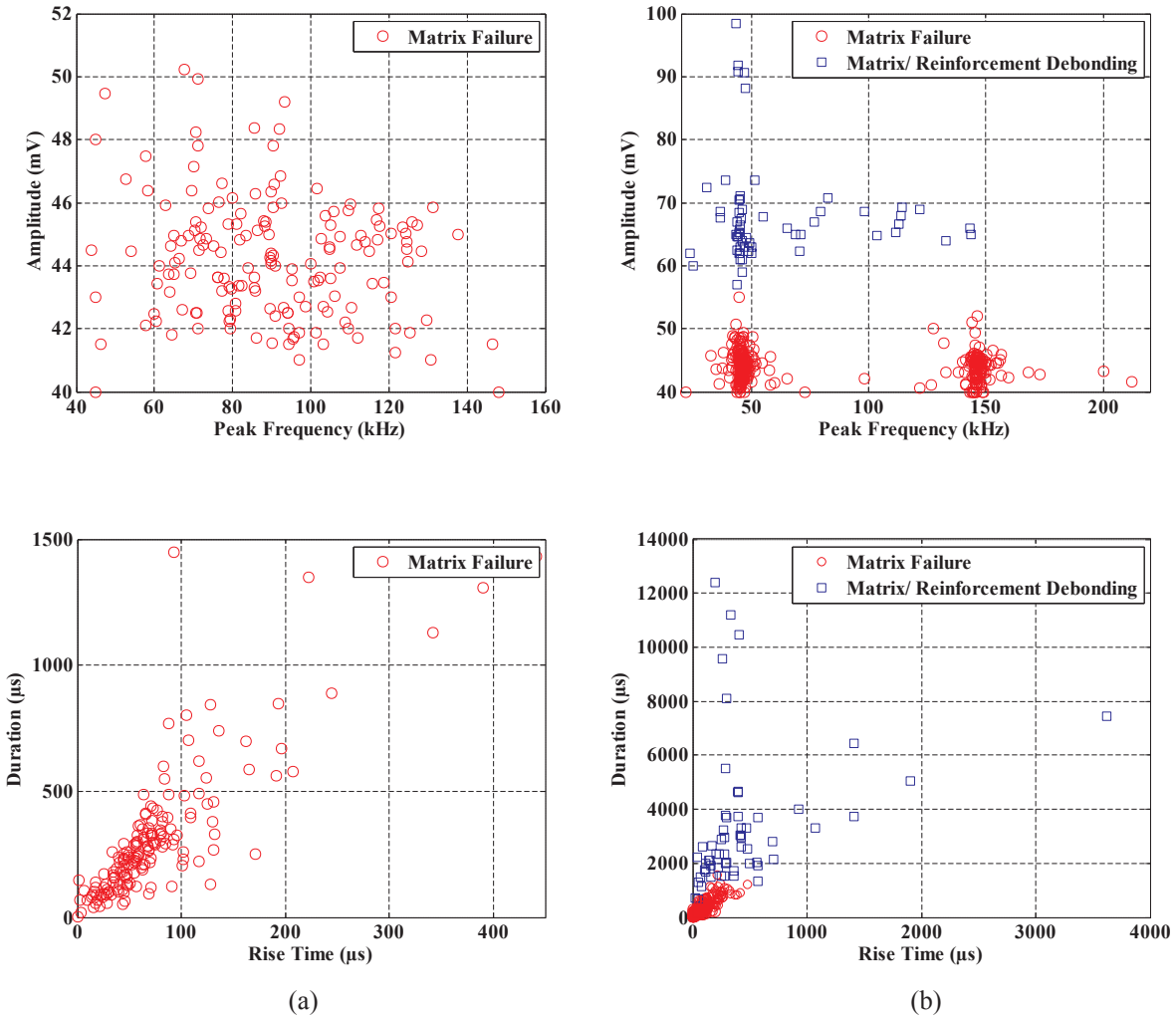

Fig. 13. Distribution patterns of peak frequency vs. amplitude and rise time vs. duration: (a) RC Beam, (b) SFRC Beam.

between the maximum AE cumulative energy of RC Beam and SFRC Beam can easily be detected. For RC Beam, the final AE energy approximately reaches to $7.2x10^4$ aJ, while this value for SFRC Beam is about $1.4x10^4$ aJ which means that the total AE energy released by the SFRC Beam has a significant decrease. This result is in agreement with Aggelis et al. [44] concerning increasing of the toughness with the amount of the steel fiber increase and decreasing of AE energy with the increase in toughness.

As clearly seen in Fig. 15a, at times when the longitudinal reinforcement yielded and the RC Beam lost its load bearing capacity, significant AE energies were released and related sudden increases can be spotted. After the first sudden increase in RC Beam, the structure lost the major part of its load bearing capacity since no other sudden increases in cumulative AE energy occurred until the last one, which afterward, the structure completely lost its load bearing capacity and culminated to its failure point. However, in the SFRC Beam, no fluctuations in AE energy were observed and the graph increased gradually (Fig. 15b). This phenomenon is interpreted by Behnia et al. [28] as mechanisms supported by steel fibers do not cause sudden AE activities after cracking of concrete due to bridging mechanism of the steel fibers.

6. Conclusions

In this study, two reinforced concrete beams, one of which included steel fibers within the concrete matrix, were tested under three-point-bending and monitored by acoustic emission (AE) technique. In order to characterize the steel fiber/matrix de-bonding apart from concrete matrix cracking sources, cluster analyses were applied to AE data. Cracking strength, yielding load capacity and ultimate load capacity of SFRC Beam were obtained 87%, 33% and 39% higher than those of RC Beam, respectively. In this way, it was demonstrated that presence of the steel fiber in concrete enhances the structural performance of the reinforced concrete beam under bending.

Clustering is a promising technique to characterize steel fiber/concrete matrix de-bonding mechanism apart from cracking of the

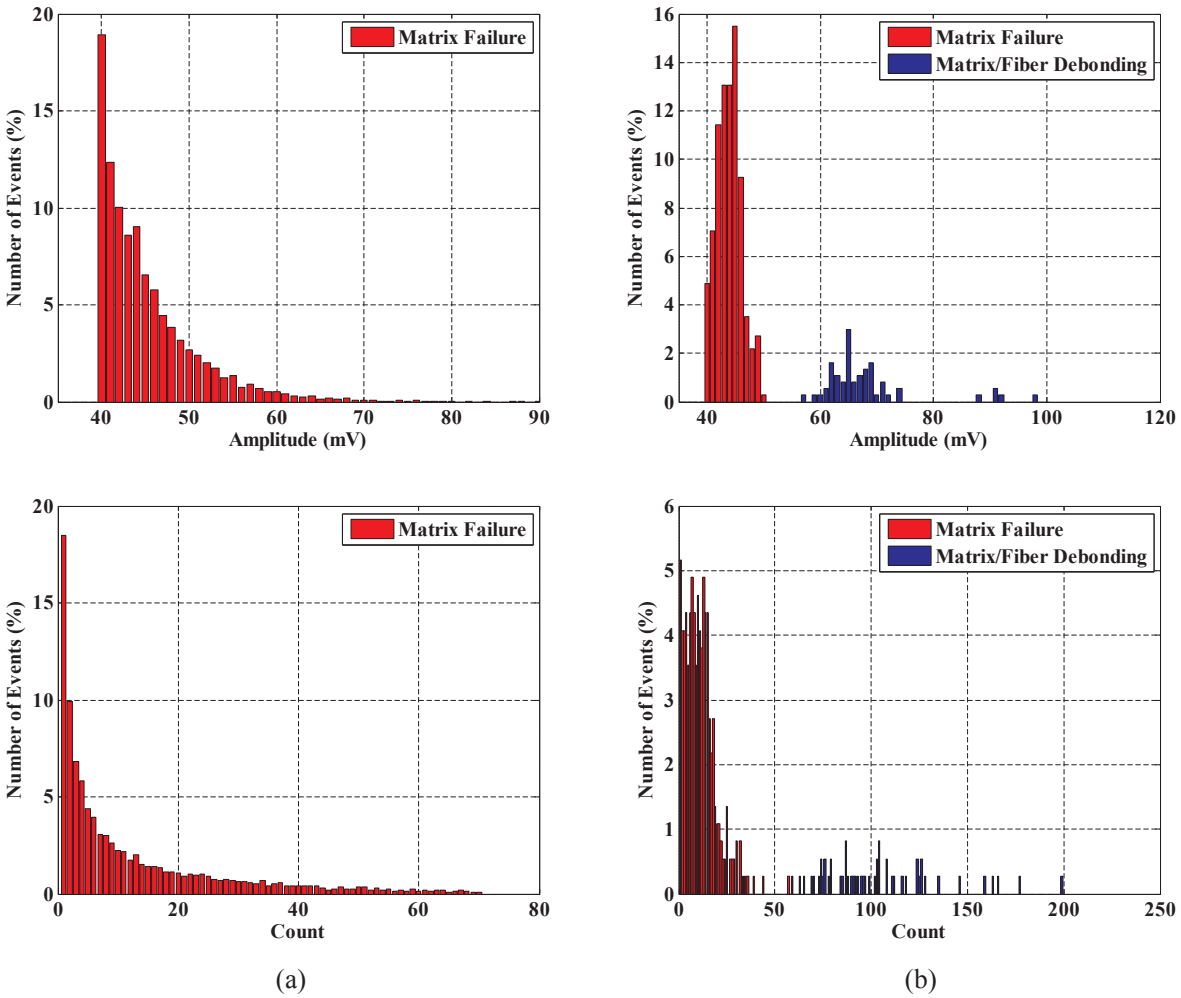

Fig. 14. Magnitude ranges of the acoustic emission features: (a) RC Beam, (b) SFRC Beam.

Table 3
Mean values of the acoustic emission features.

Test Specimen	Failure Mechanism	Rise Time (μs)	Count	Duration	Amplitude (μs)	RMS	Abs-Energy (aJ)
RC Beam	Cluster 1 (Matrix Failure)	152.3	23.17	573.3	45.16	0.0018	5714.1
		0–200	0–50	0–1500	40–52	2×10^{-4} – 0.3674	0 – 3,270,000
SFRC Beam	Cluster 1 (Matrix Failure)	110.87	13.13	417.17	44.47	0.0042	2121.03
		0–500	0–50	0–1500	40–55	2×10^{-4} – 1.4430	0 – 3,270,000
	Cluster 2 (De-bonding)	425.54	144.61	4162.3	70.8	0.0905	1.2194×10^{7}
		100–2000	50–350	700–12000	55–100	2×10^{-4} – 1.4776	3192 – 341,587,000

concrete. By conducting “k-means” algorithm, effect of presence of the steel fiber within concrete was clearly distinguished due to revealing two types of clusters as concrete matrix failure and steel fiber/matrix de-bonding. Thus, it was proved that *k*-means is an effective method to clarify steel fiber/matrix de-bonding mechanism.

After evaluating the relative distributions of AE features, it was shown that “rise time vs. count” and “duration vs. amplitude” distribution patterns have the highest capability in determining the failure status of the concrete and steel fiber reinforced concrete, while it is not possible to make a distinction using “peak frequency vs. amplitude” and “rise time vs. duration” distribution patterns. Total AE energy released by the plain reinforced concrete beam is higher than the steel fiber reinforced concrete beam. This is because the mechanisms supported by steel fibers do not cause sudden AE activities after cracking of concrete due to bridging mechanism of the steel fibers.

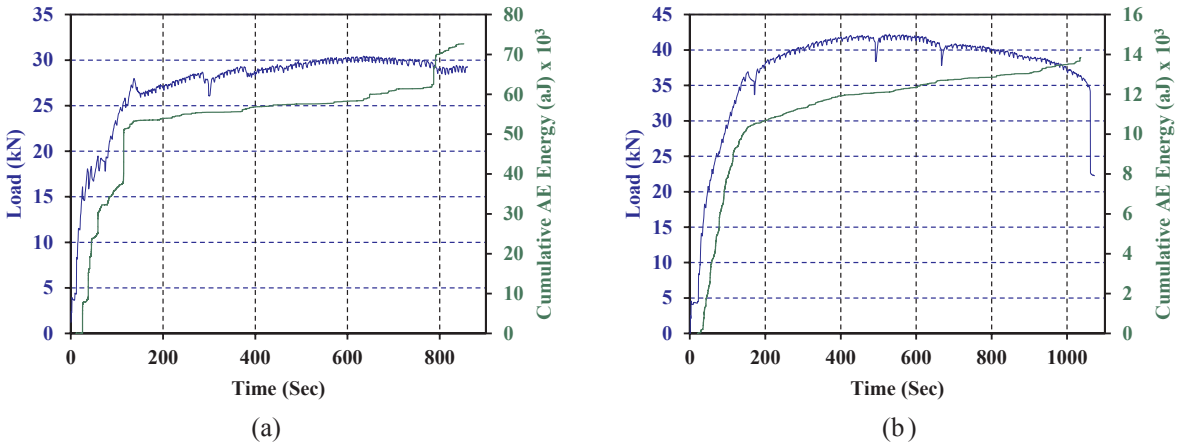

Fig. 15. Time vs AE cumulative energy and load: (a) RC Beam, (b) SFRC Beam.

Acknowledgements

Financial support provided by TUBITAK (The Scientific and Technological Research Council of Turkey) to conduct this experimental research under the grant number 112M822 is greatly acknowledged.

Appendix A. Supplementary material

Supplementary data associated with this article can be found, in the online version, at http://dx.doi.org/10.1016/j.engfracmech.2018.03.007.

References

[1] Slater E, Moni M, Alam MS. Predicting the shear strength of steel fiber reinforced concrete beams. Constr Build Mater 2012;26:423–36.
[2] Buratti N, Mazzotti C, Savoia M. Post-cracking behaviour of steel and macro-synthetic fibre-reinforced concretes. Constr Build Mater 2011;25:2713–22.
[3] Abdul-Ahad RB, Aziz OQ. Flexural strength of reinforced concrete T-beams with steel fibers. Cem Concr Compos 1999;21:263–8.
[4] Lu Y, Li N, Li S, Liang H. Behavior of steel fiber reinforced concrete-filled steel tube columns under axial compression. Constr Build Mater 2015;95:74–85.
[5] Afroughsabet V, Ozbakkaloglu T. Mechanical and durability properties of high-strength concrete containing steel and polypropylene fibers. Constr Build Mater 2015;94:73–82.
[6] Mertol HC, Baran E, Bello HJ. Flexural behavior of lightly and heavily reinforced steel fiber concrete beams. Constr Build Mater 2015;98:185–93.
[7] Yoo DY, Banthia N, Kim SW, Yoon YS. Response of ultra-high-performance fiber-reinforced concrete beams with continuous steel reinforcement subjected to low-velocity impact loading. Compos Struct 2015;126:233–45.
[8] Wang ZL, Wu LP, Wanh JG. A study of constitutive relation and dynamic failure for SFRC in compression. Constr Build Mater 2010;24:1358–63.
[9] Michels J, Christen R, Waldmann D. Experimental and numerical investigation on postcracking behavior of steel fiber reinforced concrete. Engng Fract Mech 2013;98:326–49.
[10] Sahoo DR, Maran K, Kumar A. Effect of steel and synthetic fibers on shear strength of RC beams without shear stirrups. Constr Build Mater 2015;83:150–8.
[11] Mindess S, Handbook of Nondestructive Testing of Concrete, V.M. Malhotra, N.J. Carino, (Eds.), CRC Press 2004.
[12] Soulioti D, Barkoula NM, Paipetis A, Matikas TE, Shiotani T, Aggelis DG. Acoustic emission behavior of steel fibre reinforced concrete under bending. Constr Build Mater 2009;23:3532–6.
[13] Anastasapoulos A, Tsimogiannis A, Toutountzakis T, Papanicolau C, Triantafillou T. Non destructive testing of reinforced concrete beams using acoustic emission, The 5th national conference of the hellenic society for non-destructive testing "non-destructive testing: certification, applications, new developments, november 18–19. Athens: Greece; 2005.
[14] Gollob S, Vogel T. Localisation of Acoustic Emission in Reinforced Concrete Using Heterogeneous and Orthotropic Velocity Models, The 10th fib International PhD Symposium in Civil Engineering, Quebec, Canada, 2014 375–380.
[15] Kocur GK, Vogel T. Classification of the damage condition of preloaded reinforced concrete slabs using parameter-based acoustic emission analysis. Constr Build Mater 2010;24:2332–8.
[16] Mirmiran A, Philip S. Comparison of acoustic emission activity in steel-reinforced and FRP-reinforced concrete beams. Constr Build Mater 2000;14:299–310.
[17] Ogawa Y, Kawasaki Y, Okamoto T. Fracture behaviour of RC members subjected to bending shear and torsion using acoustic emission method. Constr Build Mater 2014;67:165–9.
[18] Ohtsu M, Ohtsuka M. Damage Evaluation by AE in the Fracture Process Zone of Concrete, J Materials, Concrete Structures Pavement, JSCE, 599/V-40, 1998 177–184.
[19] Ohno K, Ohtsu M. Crack classification in concrete based on acoustic emission. Constr Build Mater 2010;24(12):2339–46.
[20] Aggelis DG. Classification of cracking mode in concrete by acoustic emission parameters. Mech Res Commun 2011;38(3):153–7.
[21] Alver N, Tanarslan HM, and Tayfur S. Monitoring fracture processes of CFRP-strengthened RC beam by acoustic emission. Journal of Infrastructure Systems. 23, 1, B4016002:1–9 2017.
[22] Jain AK. Data clustering: 50 years beyond K-means. Pattern Recogn Lett 2010;31:651–66.
[23] Malinen MI, and Istodor-Mariescu R, Fränti. K-means: Clustering by gradual data transformation. 47, 10, 2014 3376–3386.
[24] Manson G, Worden K, Holford K, Pullin R. Visualisation and dimension reduction of acoustic emission data for damage detection. J Intell Mater Syst Struct 2002;12:529–36.
[25] Eaton MJ, Pullin R, Hensman JJ, Holford KM, Worden K, Evans SL. Principal component analysis of acoustic emission signals from landing gear components: an aid to fatigue fracture detection. Internat J Exp Mech 2011;47(S1):588–94.
[26] Islam MS, Alam S. Principal component and multiple regression analysis for steel fiber reinforced concrete (SFRC) beams. Internat J Concrete Struct Mater

2013;7(4):303–17.
[27] Heidary H, Karimi NZ, Ahmadi M, Rahimi A, Zucchelli A. Clustering of acoustic emission signals collected during drilling process of composite materials using unsupervised classifiers. J Compos Mater 2015;49(5):559–71.
[28] Behnia A, Chai HK, Ranjbar N, Jumaat MZ. Damage detection of SFRC concrete beams subjected to pure torsion by integrating acoustic emission and Weibull damage function. Structural Control Health Monitoring 2016;23(1):51–68.
[29] Golinval J-C. Damage detection in structures based on principal component analysis of forced harmonic responses. Procedia Engng 2017;199:1912–8.
[30] Rossiter JA. Analysis and prediction of properties of concrete and its component [Masters by Research thesis]. Queensland University of Technology; 1993.
[31] Godin N, Huguet S, Gaertner R, Salmon L. Clustering of acoustic emission signals collected during tensile tests on unidirectional glass/polyester composite using supervised and unsupervised classifiers. NDT E Int 2004;37(4):253–64.
[32] Ning A, Jun X, Xiaohua Z, and Xiaoni G. Application of PCA in concrete infrared thermography detection. 2nd International Workshop on Materials Engineering and Computer Sciences 2015.
[33] Milovanovic B, and Pecur IB. Principle component thermography for defect detection in reinforced concrete structures, Advances in Cement and Concrete Technology in Africa, Tanzania, Advances in Cement and Concrete Technology in Africa. Proceedings 2nd International Conference, January 2016.
[34] Calabrese L, Campanella G, Proverbio E. Use of cluster analysis of acoustic emission signals evaluating damage severity in concrete structures. J Acoust Emission 2010;28:129–41.
[35] Calabrese L, Campanella G, Proverbio E. Identification of corrosion mechanisms by univariate and multivariate statistical analysis during long term acoustic emission monitoring on a pre-stressed concrete beam. Corros Sci 2013;73:161–71.
[36] Saliba J, Loukili A, Grondin F, Regoin JP. Identification of damage mechanisms in concrete under high level creep by the acoustic emission technique. Mater Struct 2014;47(6):1041–53.
[37] Fotouhi M, Sadeghi S, Jalalvand M, Ahmadi M. Analysis of the damage mechanisms in mixedmode delamination of laminated composites using acoustic emission data clustering. J Thermoplast Compos Mater 2017;30(3):318–40.
[38] Anay R, Soltangharaei V, Assi L, DeVol T, Ziehl P. Identification of damage mechanisms in cement paste based on acoustic emission, Construction and Building Materials Roundi, W., El Mahi, A., El Gharad, A. and Rebiere, J.-L., 2018, Acoustic emission monitoring of damage progression in glass/epoxy composites during static and fatigue tensile tests, Applied Acoustics. 2018 132, 124–134, 164, 286–296 pp .
[39] Roundi W, El Mahi A, El Gharad A, Rebiere J-L. Acoustic emission monitoring of damage progression in glass/epoxy composites during static and fatigue tensile tests. Appl Acoust 2018;132:124–34.
[40] ASTM E1316, Standard Terminology for NDT, 2002.
[41] Jolliffe IT. Principal Component Analysis. Second Edition New York: Springer-Verlag; 2002.
[42] Kaufman, L., Rousseeuw, P. J., 2008, Finding Groups in Data: An Introduction to Cluster Analysis, John Wiley&Sons.
[43] Rousseeuw PJ. Silhouettes: a graphical aid to the interpretation and validation of cluster analysis. Computat Appl Mathemat 1987;20:53–65.
[44] Aggelis DG, Soulioti DV, Gatselou EA, Barkoula N-M, Matikas TE. Monitoring of the mechanical behavior of concrete with chemically treated steel fibers by acoustic emission. Constr Build Mater 2013;48:1255–60.